APPLIED PHYSICS LETTERS VOLUME 72, NUMBER 18 4 MAY 1998

Demonstration of Si homojunction far-infrared detectors

A. G. U. Perera^{a)} and W. Z. Shen

Department of Physics and Astronomy, Georgia State University, Atlanta, Georgia 30303

H. C. Liu and M. Buchanan

Institute for Microstructural Sciences, National Research Council, Ottawa K1A 0R6, Canada

M. O. Tanner and K. L. Wang

Department of Electrical Engineering, University of California at Los Angeles, Los Angeles, California 90095

(Received 16 February 1998; accepted for publication 5 March 1998)

A 48 μ m cutoff wavelength (λ_c) Si far-infrared (FIR) detector is demonstrated. Internal photoemission over a Si interfacial work-function of a homojunction consisting of molecular beam epitaxy grown multilayers (p^+ emitter layers and intrinsic layers) is employed. The detector shows high responsivity over a wide wavelength range with a peak responsivity of 12.3 ± 0.1 A/W at 27.5 μ m and detectivity D^* of 6.6×10^{10} cm \sqrt{Hz} /W. The λ_c and bias dependent quantum efficiency agree well with theory. Based on the experimental results and the model, Si FIR detectors (40–200 μ m) with high performance and tailorable λ_c s can be realized using higher emitter layer doping concentrations. © 1998 American Institute of Physics. [S0003-6951(98)03818-2]

High performance far-infrared (40–200 μ m) semiconductor detectors as well as large focal plane arrays are required for space astronomy applications, such as NASA's Space Infrared Telescope Facility (SIRTF) program. Present far-infrared (FIR) detectors used or under development for that wavelength range are extrinsic Ge photoconductors (unstressed or stressed)² and Ge block-impurity-band (BIB) detectors,³ nevertheless, there are many technological challenges for fabricating large format arrays in germanium.² Since almost all the circuit components are fabricated using mainstream Si technology, incorporating different components in a single chip to fabricate an integrated circuit (IC) is a major advantage of using Si. In addition, high uniformity and advances in monolithic integration technology of Si can play an important role in developing focal plane arrays. However, at present, no Si FIR detectors exist that can operate effectively beyond 40 μ m at low background.⁴ Recently, an analytical model was presented⁵ for Si homojunction interfacial work-function internal photoemission (HIWIP) FIR detector, which shows high performance and tailorable cutoff wavelength λ_c . The main significance of this detector concept is in establishing a technology base for the evolution of high performance, large area, uniform detector arrays using the well established Si growth and processing technology.

The basic structure of HIWIP detectors consists of a heavily doped emitter layer and an intrinsic layer across which most of the external bias is dropped. The detection mechanism involves infrared absorption in the emitter layer followed by the internal photoemission of photoexcited carriers across the junction barrier and then collection. λ_c (μ m) is defined as 1.24/ Δ (eV), where Δ is the work function. Depending on whether the doping concentration is below or above the metal-insulator transition (Mott transition) value, the work function is the energy gap between the impurity

band and the conduction (valence) band or interfacial barrier between the intrinsic layer and the Fermi level in the emitter layer as defined before⁵ (different from the vacuum level to Fermi level). One of the unique features is that, in principle, Si FIR detectors can be designed with arbitrary long λ_c , since Δ can become arbitrary small with increased doping concentrations. Here the realization of this novel Si HIWIP FIR detector is reported with doping concentration below the Mott transition concentration as the foundation towards achieving $\lambda_c \sim 200~\mu m$ Si HIWIP detectors.

The sample was grown by molecular beam epitaxy (MBE) at 700 °C on p-type Si(100) substrate with resistivity of 18–22 Ω cm. The MBE epilayers consist of a 7740 Å bottom contact (p^{++}) layer, a 3870 Å undoped i layer, 10 periods of 645 Å emitter (p^{+}) layers and 1290 Å undoped i layers, and finally, a 3870 Å top emitter layer and a 5160 Å top contact layer as shown in Fig. 1. Multilayers were used to increase the quantum efficiency due to the increased photon absorption efficiency and possible photocur-

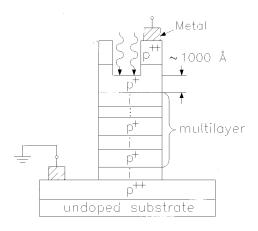


FIG. 1. Schematic of the p-Si multilayer HIWIP detector after device processing. p^{++} , p^+ and i are the contact layer, emitter layer and undoped layer, respectively. A window is opened on the top side for frontside illumination.

a)Electronic mail: phyuup@panther.gsu.edu

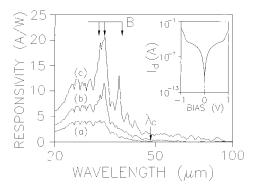


FIG. 2. Spectral response of p-Si HIWIP FIR detector measured at 4.2 K under different forward (top positive) bias V_b (a) 0.377 V, (b) 0.539 V, and (c) 0.791 V. A peak responsivity of 12.3 A/W is observed at 27.5 μ m in curve (c). The spike responses are associated with excited impurity states with the theoretical energy levels marked by arrows. The other minor features are due to the instrument response function against which the detector output was ratioed. The inset shows the dark current I_d vs V_b of the detector at 4.2 K.

rent gain enhancement.⁵ The emitter layers were doped with Boron to 2.0×10^{18} cm⁻³. The top and bottom contact layers were doped to 2×10^{19} cm⁻³, above the Mott transition value of 1.47×10^{19} cm⁻³ for p-Si⁵ to ensure an ohmic contact. Thickness and the concentration control of MBE growth is confirmed by the spreading resistance measurements. The contact was formed by deposition of Al and the optical window area (A_0) is $260 \times 260 \ \mu\text{m}^2$. The p-Si HIWIP FIR detector was characterized by current–voltage (I-V) measurements and photoresponse. The responsivity was obtained using a Perkin–Elmer, system 2000, Fourier transform infrared spectrometer (FTIR) and a Si composite bolometer as the reference.

Figure 2 shows the spectral response at 4.2 K measured at different forward biases for the 10-layer p-Si HIWIP sample. A wide spectrum with high responsivity is obtained. The long tailing behavior in the long wavelength reflects the nature of internal photoemission. The responsivity has a strong bias dependence, increasing significantly with increasing bias. However, the bias cannot increase indefinitely as the dark current also increases with bias. The spectral response at reverse biases is similar to that at forward biases.

It is noted that several spikes (associated with excited impurity states) appear in the spectra under high biases, which becomes stronger with increasing bias. At low biases, the photoconductivity is due to the usual photon capture by the impurity states, where λ_c of the response is determined by the energy gap Δ . At high biases, under suitable doping concentration where the wave function of excited impurity states overlaps, the onset of hopping conduction is observed due to the charge transport (by charge hopping) among ionized dopant sites. The recombination process mainly displays the capture of carriers by excited impurity states back to ground states, resulting in the longer λ_c s. The spike response positions are in good agreement with the theoretical energies of transitions from the ground states to the first $(2P_0)$, second $(3P_0)$ and third $(4P_0)$ excited states (marked by arrows in Fig. 2). The λ_c is 48 μ m at low biases, increasing to around 91 µm at a bias of 0.791 V. The level where the signal reaches the noise level (standard deviation of the curve) of the spectrum is determined as λ_c . The highest

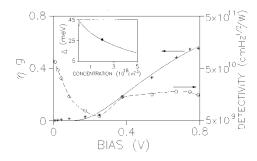


FIG. 3. Bias dependence of the measured quantum efficiency and gain product ηg (*) and detectivity (open circles). The solid curve for ηg gives the calculated results. The inset shows the Δ vs the concentration estimated by the TB model (solid curve), and an experimental point indicated by a solid circle

responsivity obtained here is 12.3 ± 0.1 A/W at $27.5~\mu m$ (in the flat region), and 20.8 ± 0.1 A/W at $31.4~\mu m$ (in the spike region). Hopping conduction can be clearly seen in the I-V data in the inset of Fig. 2, where the dark current increases rapidly with bias above 0.75~V. Since this is independent of photon flux and can reduce the sensitivity of the detector, the discussion is limited to the results of the flat region of the response and low bias case.

The current responsivity is given by

$$R = q \, \eta g / h \, \nu, \tag{1}$$

where η is the quantum efficiency and g is the photoconductive gain. The effective quantum efficiency is a product of collection efficiency (η_c , coming from absorption and diffusion of carriers) of holes flowing into i region and barrier tunneling probability (η_b):

$$\eta = \eta_c \cdot \eta_b \,. \tag{2}$$

The collection efficiency can be estimated by taking into account the absorption in emitter layers and the transport probability determined by the diffusion length. By assuming a constant absorption coefficient α and a constant diffusion length L_d (typically 1000–2000 Å) for an emitter layer of thickness d with 2(N+1) optical passes due to N-layer structures, η_c can be written as:

$$\eta_c = \{1 - \exp[-2(N+1)\alpha d]\} \exp(-d/L_d)$$

$$\approx 2(N+1)\alpha d \exp(-d/L_d), \tag{3}$$

while the tunneling probability is given by assuming a triangular barrier:

$$\eta_b = \exp \left[-\frac{4\sqrt{2m_h^*}(\Delta E_v)^{3/2}}{3g\hbar F} \right],$$
(4)

where m_h^* is the tunneling hole effective mass, ΔE_v is the offset of the valence band edge of the p^+ -i interface, and F is the electric field across the intrinsic region. The peak absorption coefficient can be obtained by $\alpha = N_a \cdot \sigma_p$, where σ_p is the peak photoionization cross section given by ⁵

$$\sigma_p = \frac{1}{\sqrt{\epsilon_s}} \cdot \frac{3.52 \times 10^{-17}}{m_d \Delta} (\text{cm}^2).$$
 (5)

Figure 3 shows the bias dependent peak quantum efficiency and gain product ηg (asterisks) at 27.5 μ m. The maximum ηg of the present detector is 0.56. It can be seen that the

above model agrees well with the experimental results with the following fitting parameters: $\Delta E_v = 2.55$ meV and g = 10.8

Boron is a substitutional acceptor in silicon with an energy level (E_A) of 44.4 meV⁶ at low concentrations. However, at higher doping concentrations, λ_c of the detector can be controlled by the doping concentration, since the impurity band broadens with increasing the doping concentration and its peak density of state moves towards the valence band rapidly. 10 The dependence of Δ on the concentration can be estimated by the tight binding (TB) approach when the concentration is below Mott transition value, as in the case here, by $\Delta = E_A - BW$, where BW is the band width.⁵ The valence band shift due to band gap renormalization (less than 1.0 meV) can be neglected at T=4.2 K. Above the Mott transition, Δ can be estimated by a modified high density (HD) theory. 9,10 The TB model, with the assumption of a random spatial (Poisson's) distribution of acceptors, gives the total impurity bandwidth⁵

$$BW=2|\langle J(R)\rangle|=2\int J(R)4\pi N_a R^2$$

$$\times \exp\left(-\frac{4}{3}\pi N_a R^3\right) dR,$$
(6)

where N_a is the doping concentration, R is the nearest-neighbor acceptor distance, and J(R) is the energy transfer integral given by

$$J(R) = \frac{q^2 \xi}{4\pi\epsilon_s \epsilon_0} (1 + \xi R) \exp(-\xi R), \tag{7}$$

where $\xi = (1/a_H)(E_A/R_H)^{1/2}$ with effective Bohr radius $a_H = 0.53\epsilon_s/m_d$ and effective Rydberg energy $R_H = 13.6m_d/\epsilon_s^2$ (ϵ_s is the relative dielectric constant and m_d is the effective density-of-state mass). Using the parameters for p-Si in Ref. 5, a Δ of 25.4 meV was obtained, corresponding to an IR detection threshold of about 48.8 μ m for the p-Si HIWIP detector with a concentration of 2×10^{18} cm⁻³. This is in good agreement with the experimental result of 48 μ m as seen in Fig. 2 and the inset of Fig. 3 (25.8 meV).

Using the measured responsivity, dark current and the gain g, we estimate the detectivity D^* (at 27.5 μ m) of the p-Si HIWIP FIR detector, which is also shown in Fig. 3. The highest D^* occurs at low biases, since the dark current increases rapidly with the bias. However, D^* also increases slight with the bias due to the rapid increase of responsivity, and finally decreases again due to the onset of hopping conduction. The highest specific detectivity D^* is 6.6×10^{10} cm

 $\sqrt{\text{Hz}}/\text{W}$ at 4.2 K under a bias of 10 mV. These preliminary responsivity results (responsivity of 12.3 A/W and η of 5.2% at 27.5 μ m shown in Figs. 2, 3) are comparable to the performance of 200 μ m Ge:Ga photoconductor operated at 3.0 K² with a responsivity \sim 5.2 A/W and $\eta \sim$ 7.7%. The Δ can be easily decreased by increasing the doping concentration (see the inset in Fig. 3), resulting in longer λ_c s. Furthermore, λ_c can be arbitrary long with doping concentrations above Mott transition value, where the IR absorption is mainly by free carrier absorption. Based on the modeling results, 5 the strong free carrier absorption in silicon, 11 our high performance p-GaAs (λ_c =100 μ m) HIWIP detector results, 9 and the present experimental results in Si, we believe that high performance, tailorable λ_c Si FIR detectors (40–200 μ m) can be realized using higher doping concentrations.

In summary, we have experimentally demonstrated for the first time the novel Si HIWIP FIR detector concept using MBE grown Si p^+ -i multilayer structure. Preliminary results obtained are promising and show that p-Si HIWIP detectors with their unique features, have great potential to become a competitor in FIR applications. Further work is under way to design and fabricate high doping concentration Si detectors and compare the experimental data with the modeling results to improve the detector performance.

This work was supported in part by the National Aeronautics and Space Administration under Contract No. NAG5-4950 with GSU and NSF under Grant No. DMR-95-20893 with UCLA. The authors wish to acknowledge S. G. Matsik at GSU for his technical help.

¹M. W. Werner, Infrared Phys. Technol. 35, 539 (1994).

²J. W. Berman and E. E. Haller, Infrared Phys. Technol. 35, 827 (1994), and references therein.

³ D. M. Watson, M. T. Guptill, J. E. Huffman, T. N. Krabach, S. N. Raines, and S. Satyapal, J. Appl. Phys. **74**, 4199 (1993).

⁴N. Sclar, in *Progress in Quantum Electronics* (Pergamon, New York, 1984), Vol. 9, pp. 149–257.

⁵ A. G. U. Perera, in *Physics of Thin Films*, edited by M. H. Francombe and J. L. Vossen (Academic, New York, 1995), Vol. 21, pp. 1–75.

 ⁶S. M. Sze, *Physics of Semiconductor Devices* (Wiley, New York, 1981).
 ⁷S. D. Gunapala, Ph.D thesis, University of Pittsburgh, 1985.

⁸ A. G. U. Perera, H. X. Yuan, S. K. Gamage, W. Z. Shen, M. H. Francombe, H. C. Liu, M. Buchanan, and W. J. Schaff, J. Appl. Phys. 81, 3316 (1997).

⁹ W. Z. Shen, A. G. U. Perera, H. C. Liu, M. Buchanan, and W. J. Schaff, Appl. Phys. Lett. **71**, 2677 (1997).

¹⁰ S. C. Jain, R. P. Mertens, and R. J. Van Overstraeten, in *Advances in Electronics and Electron Physics*, edited by P. W. Hawkes (Academic, New York, 1991), Vol. 82.

¹¹ A. G. U. Perera, W. Z. Shen, W. Mallard, M. O. Tanner, and K. L. Wang, Appl. Phys. Lett. **71**, 515 (1997).